Electronic Supplementary Information

Martyna Szymańska[1], Włodzimierz Czepa[1,2], Cezary Hołubowicz[3], Renata Świsłocka[4], Teresa Łuczak[1], Maciej Kubicki[1], Joanna Karpińska[3], Marta A. Fik-Jaskółka[*1] and Violetta Patroniak[*1]

[1]Faculty of Chemistry, Adam Mickiewicz University, Uniwersytetu Poznańskiego 8, 61-614 Poznań, Poland;

[2]Centre for Advanced Technologies, Adam Mickiewicz University, Uniwersytetu Poznańskiego 10, 61-614 Poznań, Poland;

[3]Faculty of Chemistry, University of Białystok, Ciołkowskiego 1, 15-245 Białystok, Poland;

[4]Faculty of Construction and Environmental Engineering, Technical University of Białystok, Wiejska 45e, 15-351 Białystok, Poland;

Table of contents

X-Ray crystallography

Table S1. Crystal data, data collection and structure refinement for complexes **1**, **2** and **3**.

	1	**2**	**3**
Formula	$C_{30}H_{24}CoN_6O_2S_2 \cdot ClO_4$	$C_{14}H_{12}CoN_6O_6S$	$C_{15}H_{16}CoN_6O_6S$
Formula weight	723.05	451.29	467.27
Crystal system	triclinic	triclinic	monoclinic
Space group	P-1	P-1	$P2_1/n$
a(Å)	9.3155(11)	7.8989(4)	9.6026(3)
b(Å)	14.393(2)	8.2818(5)	15.0545(5)
c(Å)	25.071(4)	14.9065(6)	12.9305(5)
α(°)	87.734(12)	76.014(4)	90
β(º)	85.935(11)	82.412(4)	106.652(4)
γ(°)	76.926(11)	64.538(5)	90
V(Å^3)	3265.1(8)	853.88(8)	1790.87(11)
Z	4	2	4
D_x(g cm^{-3})	1.471	1.755	1.733
F(000)	1480	458	956
μ(mm^{-1})	6.512	1.177	1.021
Reflections:			
collected	25525	6303	7622
unique (R_{int})	11714 (0.203)	3508 (0.022)	3746 (0.017)
with I>2σ(I)	3467	3049	3265
R(F) [I>2σ(I)]	0.1765	0.0354	0.0459
wR(F^2) [I>2σ(I)]	0.3656	0.0773	0.1185
R(F) [all data]	0.3152	0.0436	0.0534
wR(F^2) [all data]	0.4401	0.0816	0.1235
Goodness of fit	1.13	1.05	1.08
max/min Δρ (e·Å$^-$	1.40/-0.90	0.79/-0.33	2.19/-0.50

Table S2. Relevant geometrical parameters (Å, °) with standard uncertainties in parentheses. A, B and C are the least-squares planes of 6+5 system, C-N-N=C=C linker and phenyl/pyridine ring, respectively.

	2	**3**
Co1-N3	2.1579(19)	2.139(3)
Co1-N12	2.124(2)	2.137(3)
Co1-N15	2.1553(19)	2.163(3)
Co1-O1A	2.2497(19)	2.051(2)
Co1-O1B	2.2335(17)	
Co1-O2A	2.1626(17)	2.091(2)
Co1-O2B	2.2335(19)	
Co1-O1C		2.120(2)
N3-Co1-N15	149.08(8)	148.63(10)
N12-Co1-O2B	142.75(7)	
O1B-Co1-O2A	175.47(7)	
N12-Co1-O1A		164.98(10)
O1A-Co1-O1C		167.83(9)
A/B	2.68(10)	8.3(2)
B/C	8.11(13)	5.8(2)
A/C	10.26(9)	11.43(16)

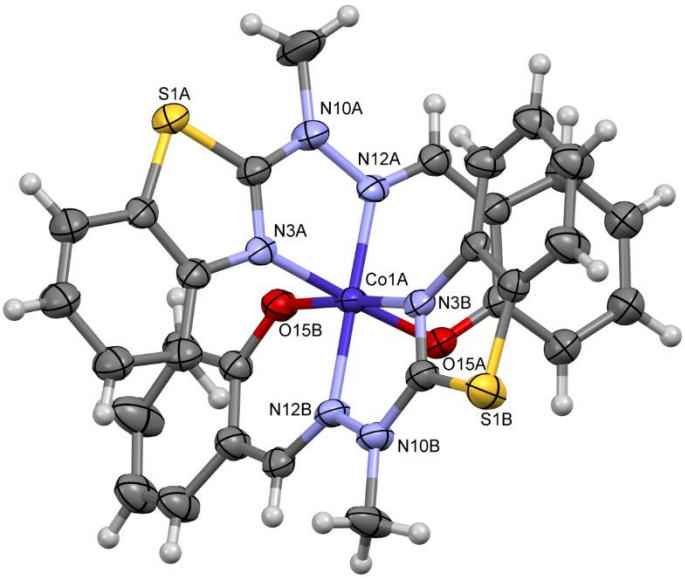

Figure S1. Perspective view of the complex **1**; ellipsoids are drawn at the 50% probability level, hydrogen atoms are represented by spheres of arbitrary radii.

Cyclic voltammetry

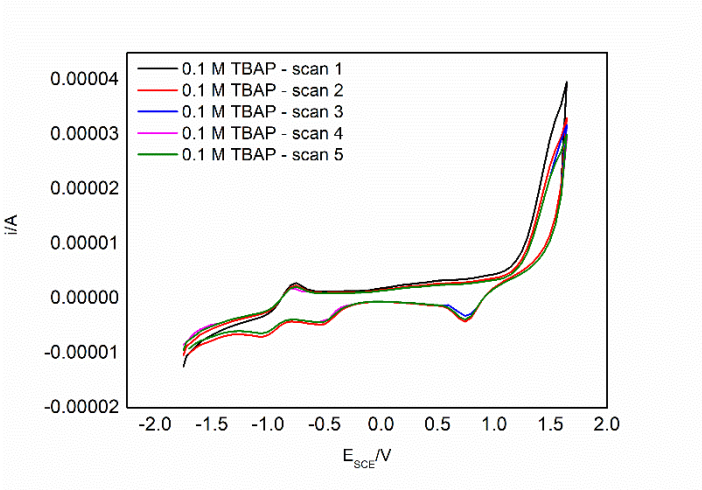

Figure S2. Cyclic voltammograms of the polycrystalline gold electrode in basic electrolyte 0.1 M TBAP in DMF. dE/dt = 0.1 V s^{-1}.

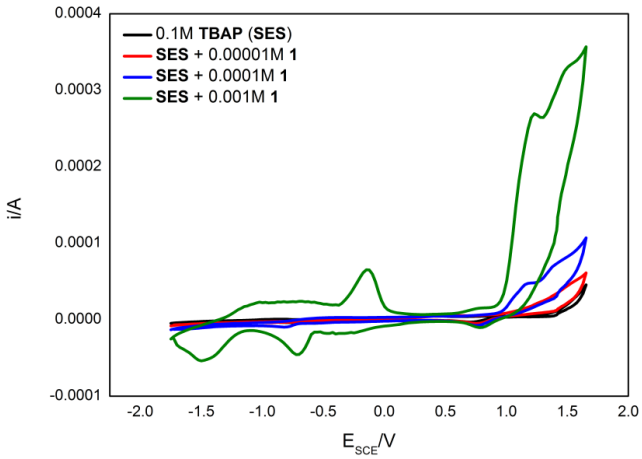

Figure S3. Cyclic voltammograms of the polycrystalline gold electrode in basic electrolyte 0.1 M TBAP in DMF and increasing amounts (10^{-5} M ÷ 10^{-3} M) of complex **1**. dE/dt = 0.1 V s^{-1}.

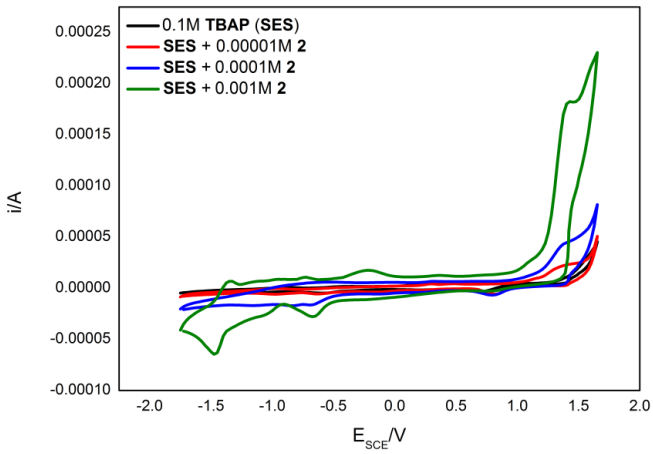

Figure S4. Cyclic voltammograms of the polycrystalline gold electrode in basic electrolyte 0.1 M TBAP in DMF and increasing amounts (10^{-5} M ÷ 10^{-3} M) of complex **2**. dE/dt = 0.1 V s^{-1}.

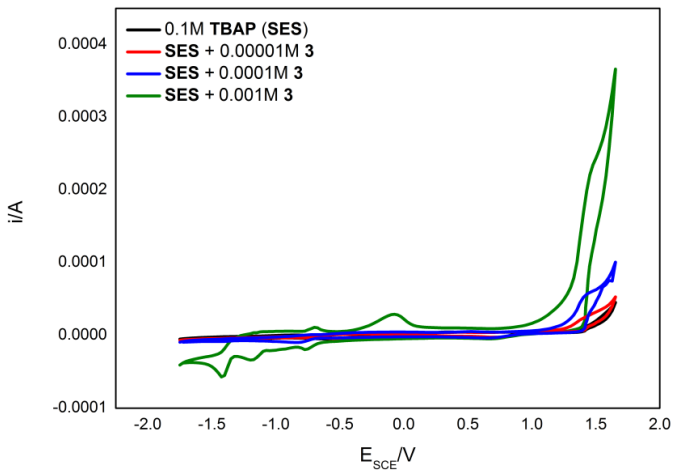

Figure S5. Cyclic voltammograms of the polycrystalline gold electrode in basic electrolyte 0.1 M TBAP in DMF and increasing amounts (10^{-5} M ÷ 10^{-3} M) of complex **3**. dE/dt = 0.1 V s^{-1}.

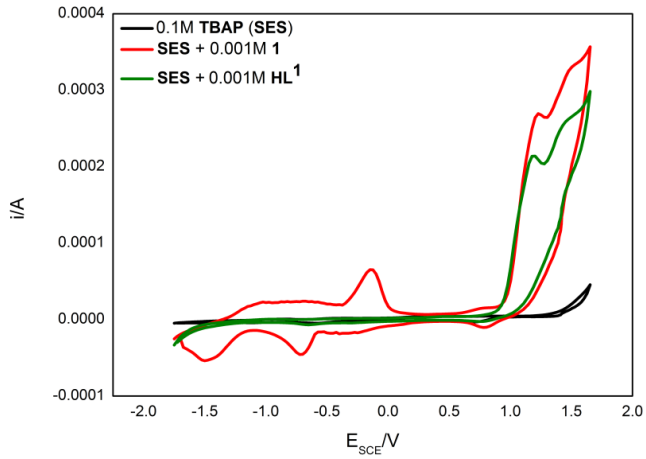

Figure S6. Cyclic voltammograms of the polycrystalline gold electrode in basic electrolyte 0.1 M TBAP in DMF and comparison of complex **1** and parent ligand **HL**^{1}. dE/dt = 0.1 V s^{-1}.

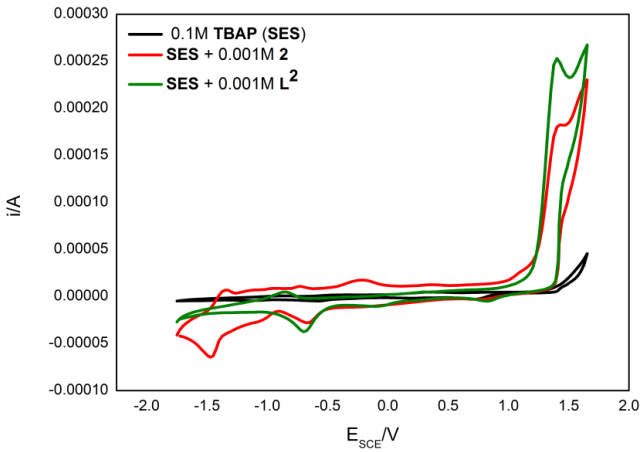

Figure S7. Cyclic voltammograms of the polycrystalline gold electrode in basic electrolyte 0.1 M TBAP in DMF and comparison of complex **2** and parent ligand **L**^{2}. dE/dt = 0.1 V s^{-1}.

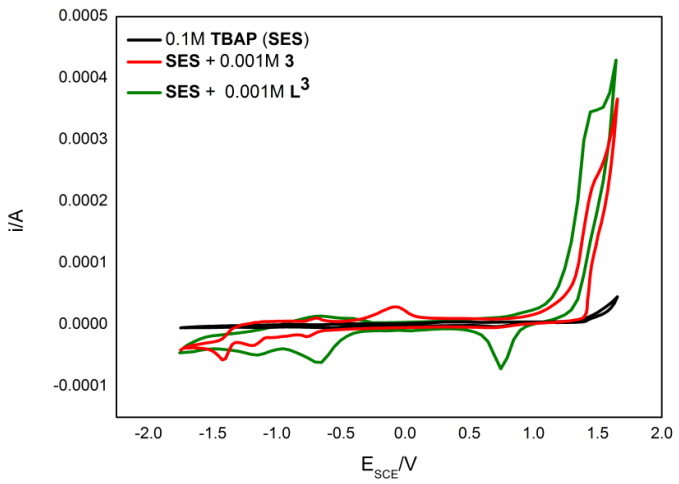

Figure S8. Cyclic voltammograms of the polycrystalline gold electrode in basic electrolyte 0.1 M TBAP in DMF and comparison of complex **3** and parent ligand $\mathbf{L^3}$. dE/dt = 0.1 V s^{-1}.

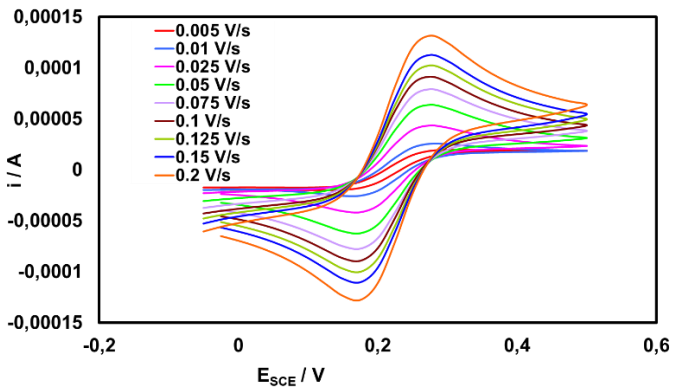

Figure S9. Cyclic voltammograms recorded at the bare polycrystalline gold electrode in 0.5 M KCl supporting electrolyte solution with $5 \cdot 10^{-3}$ M of $[Fe(CN)_6]^{4-}/[Fe(CN)_6]^{3-}$ recorded at different potential scan rates.

Photostability studies

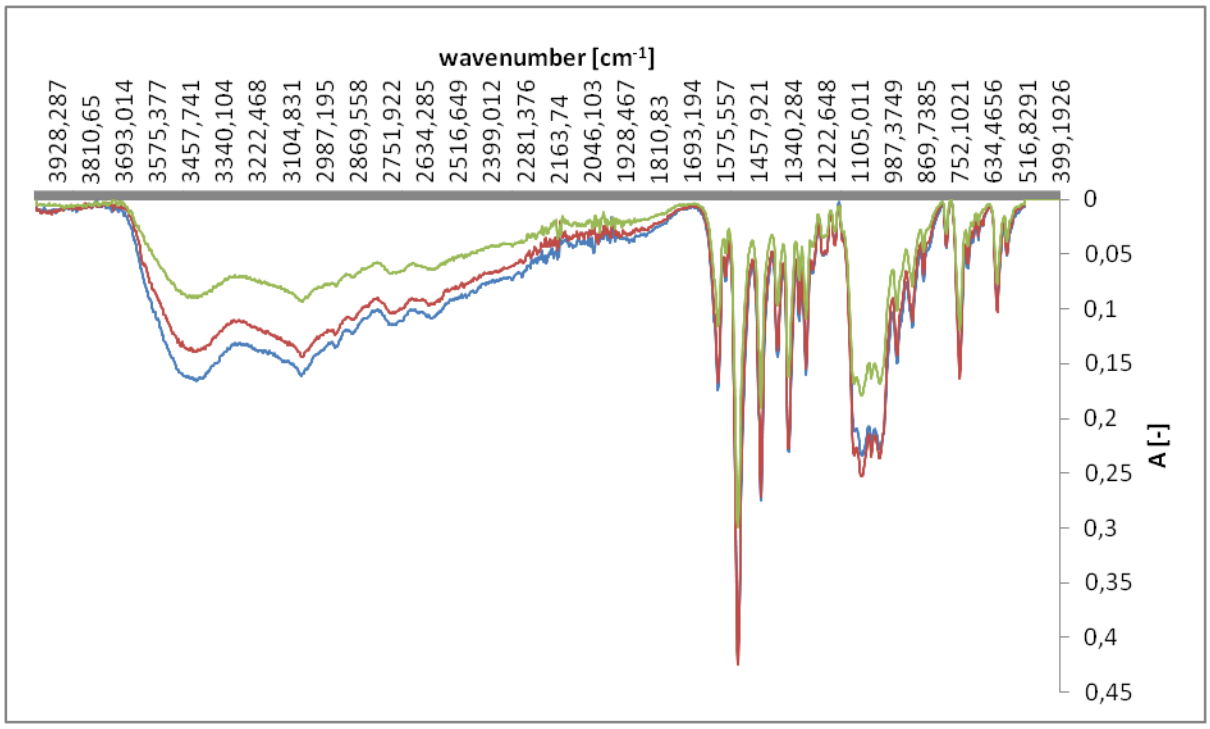

Figure S10. The FTIR spectra of complex **1** before (green line) after 120 min irradiation with UV radiation, λ = 256 nm, (blue line) or in the imaging chamber of a solar light simulator emitting light in the 300-800 nm range (red line).

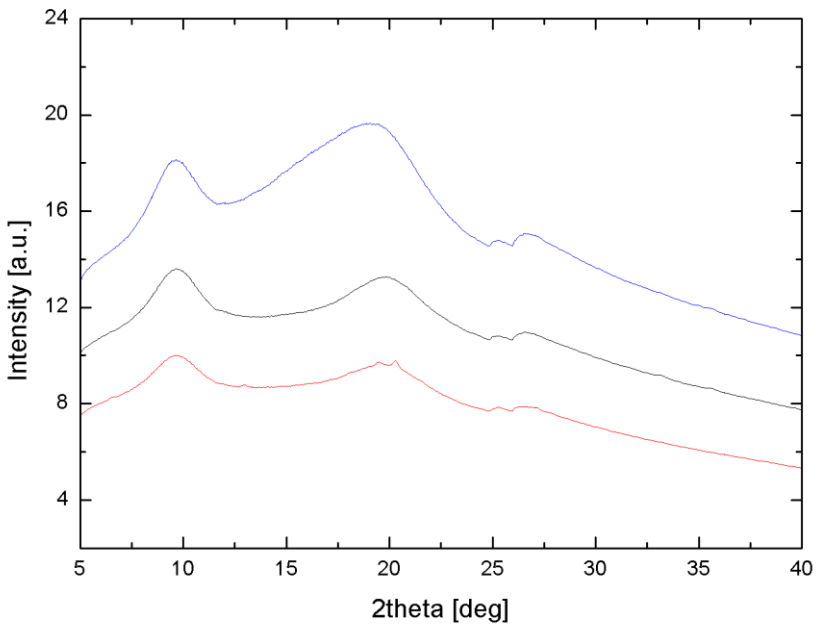

Figure S11. Observed PXRD patterns of complex **1** before (red line) and after irradiation with UV, λ = 256 nm, (blue line) or in the imaging chamber of a solar light simulator (black line).

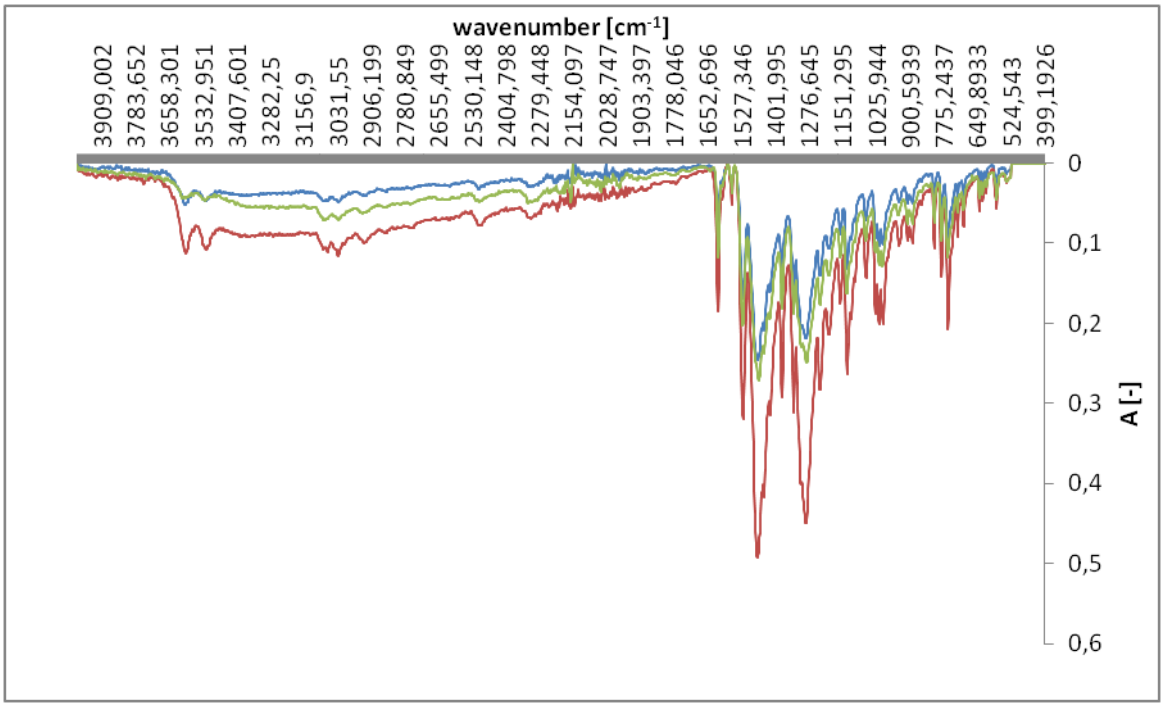

Figure S12. The FT-IR spectra of complex **2** before (green line) and after 120 min. of irradiation with UV radiation, λ = 256 nm, (blue line) or in the imaging chamber of a solar light simulator emitting light in the 300-800 nm range (red line). The irradiation showed small differences in the spectra spectrum changes in the complex **2**. A slight band change is observed at wavenumber 1464 cm^{-1}, 1468 cm^{-1} VIS, 1466 cm^{-1} UV. This band is responsible for CH_2 deformation bonds.

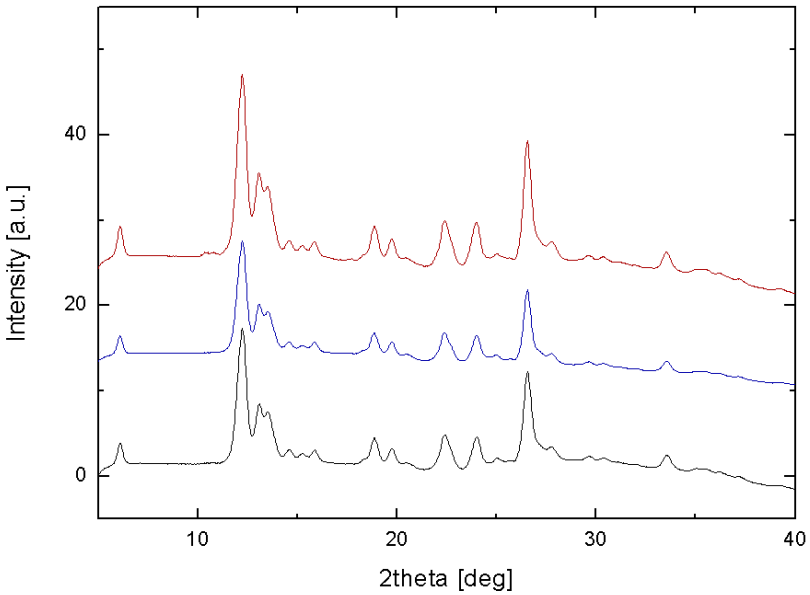

Figure S13. Observed PXRD patterns of the complex **2** before (red line) and after irradiation with UV, λ = 256 nm, (blue line) or in the imaging chamber of a solar light simulator (black line).

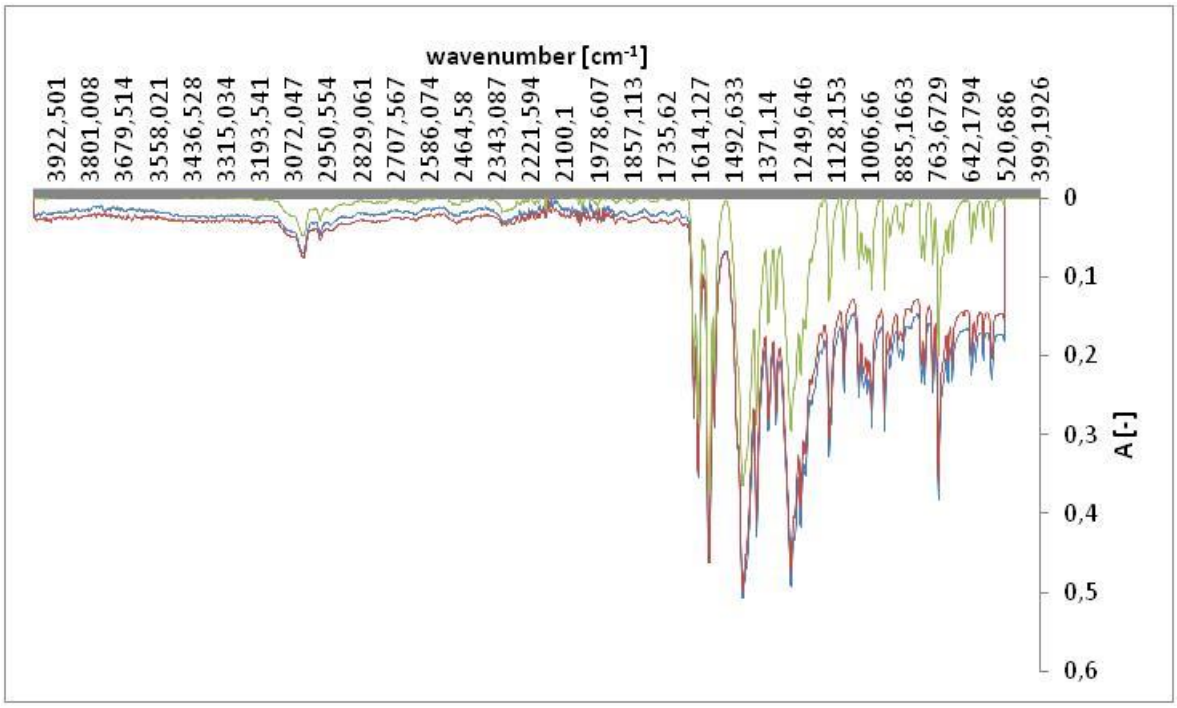

Figure S14. The FT-IR spectra of complex **3** before (green line) and after 120 min. of irradiation with UV radiation, λ = 256 nm, (blue line) or in the imaging chamber of a solar light simulator emitting light in the 300-800 nm range (red line).

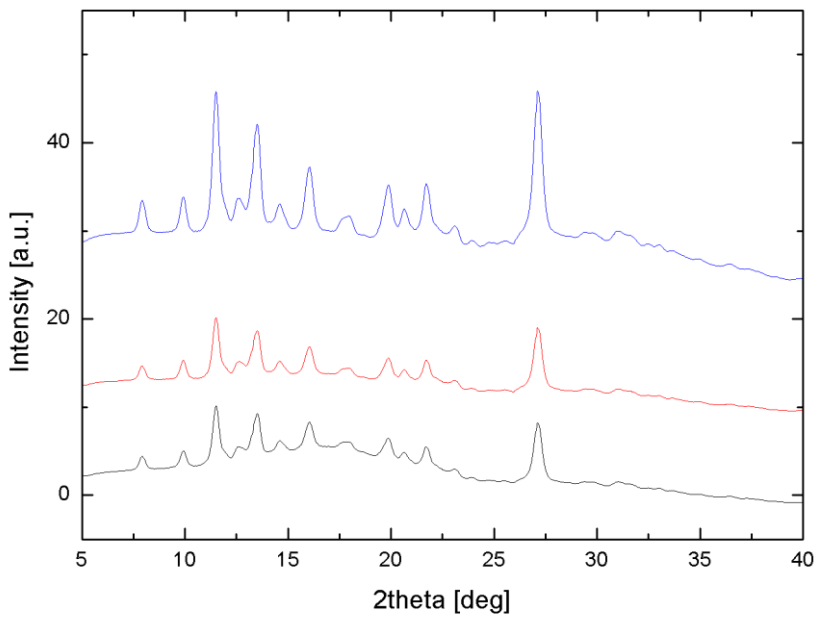

Figure S15. Observed PXRD patterns of the complex **3** before (red line) and after irradiation with UV, λ = 256 nm, (blue line) or in the imaging chamber of a solar light simulator (black line).

UV-Vis spectra of organic dyes

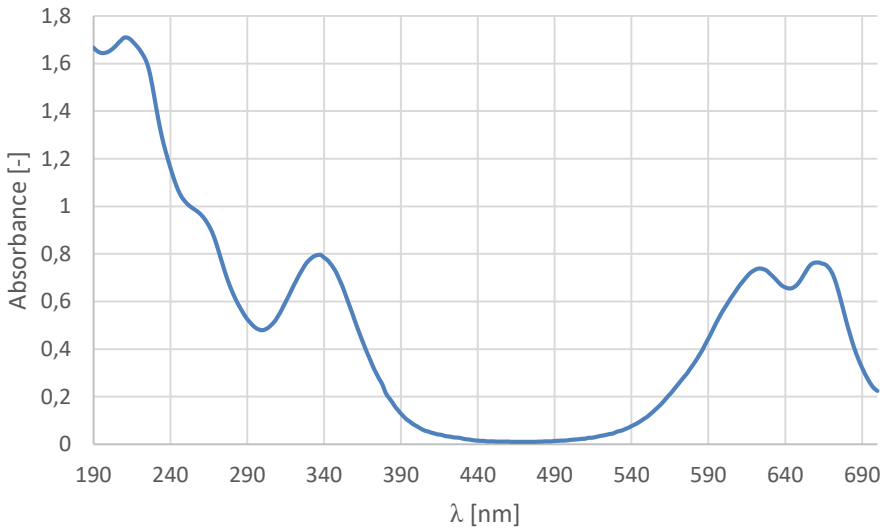

Figure S16. Absorption spectrum of Reactive Blue 21 at 50 mg/L concentration.

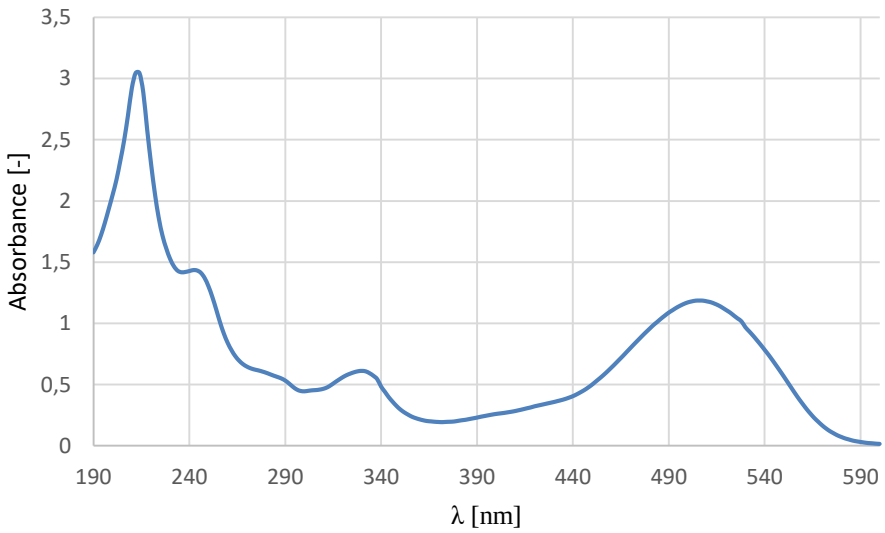

Figure S17. Absorption spectrum of Acid Red 18 at 50 mg/L concentration.